Fluorescence x-ray absorption fine structure studies of Fe-Ni-S and Fe-Ni-Si melts to 1600 K

M. H. Manghnani,* X. Hong, J. Balogh, and G. Amulele
School of Ocean and Earth Science and Technology, University of Hawaii, Honolulu, Hawaii 96822, USA

M. Sekar
Indira Gandhi Centre for Atomic Research, Tamil Nadu, Kalpakkam 603102, India

M. Newville
Consortium on Advanced Radiation Sources, University of Chicago, Chicago, Illinois 60637, USA
(Received 11 October 2007; revised manuscript received 24 March 2008; published 23 April 2008)

We report Ni *K*-edge fluorescence x-ray absorption fine structure spectra (XAFS) for $Fe_{0.75}Ni_{0.05}S_{0.20}$ and $Fe_{0.75}Ni_{0.05}Si_{0.20}$ ternary alloys from room temperature up to 1600 K. A high-temperature furnace designed for these studies incorporates two x-ray transparent windows and enables both a vertical orientation of the molten sample and a wide opening angle, so that XAFS can be measured in the fluorescence mode with a detector at 90° with respect to the incident x-ray beam. An analysis of the Ni XAFS data for these two alloys indicates different local structural environments for Ni in $Fe_{0.75}Ni_{0.05}S_{0.20}$ and $Fe_{0.75}Ni_{0.05}Si_{0.20}$ melts, with more Ni-Si coordination than Ni-S coordination persisting from room temperature through melting. These results suggest that light elements such as S and Si may impact the structural and chemical properties of Fe-Ni alloys with a composition similar to the earth's core.

DOI: 10.1103/PhysRevB.77.134110 PACS number(s): 61.05.cj, 64.70.D−, 91.35.Ed

I. INTRODUCTION

Nickel is an important alloying constituent together with iron in the earth's core and magmas, and understanding the structure of molten Fe-Ni alloys has significant geophysical implications. Nickel is expected to be found in both the inner and the outer cores, and it is an important trace element in the upper mantle, where it strongly partitions from silicate melts to coexisting minerals.[1,2] Understanding the geochemical behavior of Ni in these systems requires knowledge of its structural environment in the melts and in crystals. Mao *et al.*[3] showed experimentally that an iron-nickel alloy, $Fe_{80}Ni_{20}$, has virtually the same high-pressure compression behavior (ρ vs P relationship) as pure iron up to 300 GPa at 300 K. In addition, the presence of Ni does not significantly modify the hcp structure of pure Fe, and so it is generally concluded that the presence of Ni is safely ignored in the geophysical modeling of the core.[3,4]

The current understanding of the composition of the earth's core usually includes several wt % of light elements (O, S, and Si), though the details are a topic of active research.[5–7] The structural and chemical roles of these light elements on the Fe-Ni alloy that makes up the bulk of the earth's core are not well understood, largely due to experimental challenges of making direct, detailed structural measurements at high temperatures. Importantly, a few studies have examined the potential differences in the chemical reactivity of Fe and Ni with such light elements. In an earlier ultrasonic study, we found that liquid Fe-Ni alloy containing 8 wt % S exhibits an anomalous acoustic behavior (positive temperature dependence of compressional wave velocity),[8] which is in contrast to the normal elastic behavior of liquid Fe-Ni and Fe-Ni-Si.[1,9] The contrasting results in the temperature dependence of the elastic properties could imply structural differences in these melts. Cuello *et al.*[10] investigated the static liquid structure $S(Q)$ of one ternary Fe-Ni-S and two binary Fe-Ni iron-rich (with ~85% Fe) molten alloys by using neutron diffraction and Monte Carlo simulations. They observed that the presence of sulfur in Fe-Ni melts significantly changes the melt structure. To our knowledge, no direct structural studies of Fe-Ni-S/Si melts have been carried out.

X-ray absorption fine structure spectroscopy (XAFS) is a useful probe for determining the short-range atomic structure in structurally disordered materials.[11,12] Two inherent strengths of XAFS are that it can be measured on extremely disordered systems, such as melts, and on elements at a relatively low concentration to give the isolated structure around that selected element. To study low concentration elements, the XAFS measurement must be done in fluorescence mode, wherein the x-ray fluorescence of the absorbing element is monitored. While several furnaces have been designed and used for XAFS measurements at very high temperatures (above, say, 700 K),[13–20] only a few of these furnaces allow access to x-ray fluorescence, which is necessary for studying dilute components. This limitation has been mainly due to experimental difficulties in constructing a sample container that is suitable for holding a melt sample in a vertical orientation at extreme temperatures while also possessing large enough x-ray windows in the furnace for fluorescence measurements. While there are also some analytic challenges in interpreting the heavily damped XAFS oscillation at high temperatures, these have been largely overcome.[21–24]

For the present study, samples that have the composition $Fe_{0.75}Ni_{0.05}S_{0.20}$ and $Fe_{0.75}Ni_{0.05}Si_{0.20}$ were synthesized and studied at room temperature and at temperatures of up to 1600 K, a temperature that is estimated to be above the melting temperature for both compositions. For the S alloy, the phase diagrams of Fe-Ni and Fe-S of Kubaschewski[25] give an estimated melting temperature of 1593 K for $Fe_{0.75}Ni_{0.05}S_{0.20}$. Waldner and Pelton[26,27] estimated $Fe_{0.75}Ni_{0.05}S_{0.20}$ to be a mixed liquid+fcc phase at 1573 K

and completely liquid at 1623 K. For the Si alloy, the phase diagram of Ikeda *et al.*[28] estimated the melting temperature of $Fe_{0.80}Si_{0.20}$ to be 1608 K, with an uncertainty of 10 K. With 5% Ni, we expect the melting temperature of $Fe_{0.75}Ni_{0.05}Si_{0.20}$ to be even lower than that of $Fe_{0.80}Si_{0.20}$.

In order to facilitate such studies of the local structure of Fe-Ni-Si and Fe-Ni-S alloys in both solid and melt phases, we have developed a high-temperature furnace for fluorescence XAFS measurements. This furnace incorporates a different sample holding arrangement and allows the collection of high-quality fluorescent XAFS spectra from room temperature up to 1600 K with a fluorescence detector at 90° with respect to the incident x-ray beam. We present the furnace design and Ni *K*-edge XAFS measured for $Fe_{0.75}Ni_{0.05}S_{0.20}$ and $Fe_{0.75}Ni_{0.05}Si_{0.20}$ up to 1600 K with this furnace, and we show the local environments of Ni to be dramatically different between these two alloys.

II. EXPERIMENTAL HIGH-TEMPERATURE FURNACE FOR X-RAY ABSORPTION FINE STRUCTURE

Our primary aim in optimizing the design for a furnace for fluorescent XAFS studies on high-temperature melts was to reduce the absorption of the incident and fluoresced x rays by the furnace windows as much as possible and to keep the melt sample vertical during the measurements. To our knowledge, no transmission-mode XAFS measurements have been made on Fe-Ni samples with Ni as low as 5 wt % mainly because the Fe *K* edge is just below that of Ni (7112 eV for Fe, 8333 eV for Ni), so that the absorption from Fe will dominate the total absorption from the sample at these concentrations. In contrast, Fe-Ni alloys with 5 wt % Ni are well suited for fluorescence measurements, wherein the intensity of the Ni $K\alpha$ emission is monitored and taken to be proportional to the Ni *K*-edge absorption cross section. XAFS measurements in the fluorescence mode present their own challenges, including the presence of Fe $K\alpha$ fluorescence and the need for a large solid angle of collection due to the isotropic nature of x-ray fluorescence. This, in turn, demands large x-ray transparent windows.

Our high-temperature furnace consists of a vacuum furnace with Be and Kapton® windows and a boron nitride (BN) sample holder. It has been designed as a modification of a Leitz 1760 microscope heating stage for measurements up to 1700 K. Figure 1 gives a sketch of the side view of the vacuum furnace, and Fig. 2 shows photographs of the furnace installed in the x-ray beamline and details of the furnace design. The furnace incorporates two x-ray transparent windows, an inner Be window and an outer Kapton window, and has a large opening angle for fluorescence mode XAFS, with the x-ray fluorescence detector at 90° with respect to the incident beam. The Be window (Brush-Wellman PF-60 grade is used: 99.0% purity, with 800 ppm Fe; 25 mm in diameter and 1 mm in thickness) is located between the heater and the Kapton window and is used as the primary thermal shield, which protects the outer Kapton window from thermal radiation. The Kapton window keeps the sample under a rough vacuum and is mounted on a copper plate with a 7×20 mm^2 slot to allow incident x rays in and fluoresced x rays out. The outer copper plate is removable to facilitate changing the sample and window. Both the Be and the Kapton windows provide good x-ray transmission at the Ni *K* edge. The outer furnace is water cooled to keep the Kapton window at a relatively lower temperature. The x-ray windows are sealed by an O-ring and the furnace is kept evacuated to 10^{-3} torr.

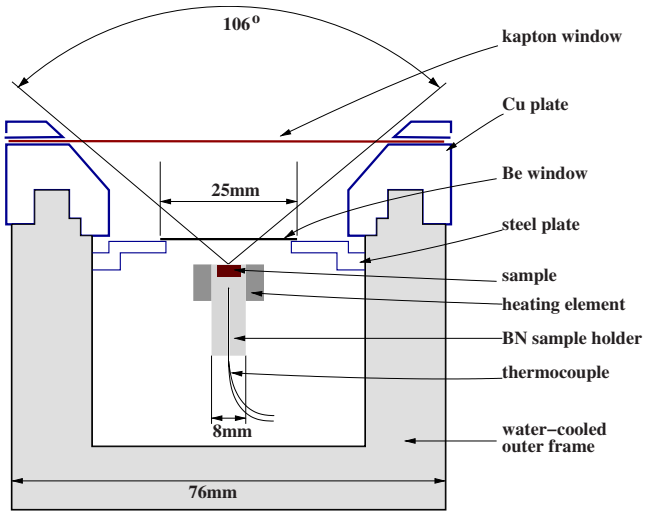

FIG. 1. (Color online) Schematic of a high-temperature furnace for fluorescence XAFS. An outer Kapton window and an inner Be window allow a large open solid angle of low *Z* material for incident x rays to get to the sample and fluoresced x rays to get from sample to detector.

The melt samples must be contained in a cell made of materials that are transparent to x rays and yet resistant to chemical corrosion by the melts. In addition, the melt

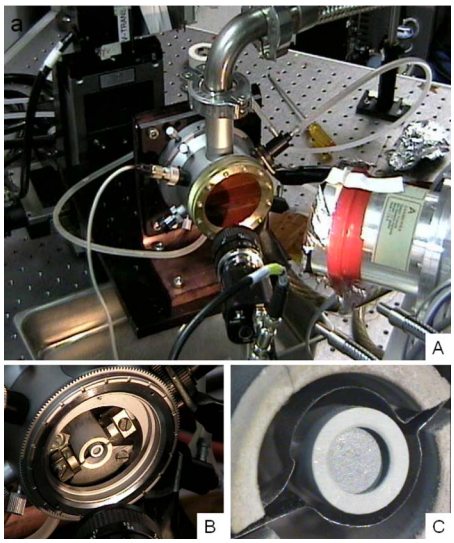

FIG. 2. (Color online) Photographs of the furnace for high-temperature fluorescent XAFS. (A) furnace installed at the x-ray beamline (APS station 13-BM-D) showing outer housing, vacuum line, water-cooling lines, and fluorescence detector to the right of the furnace. (B) Inside the furnace, with Be and Kapton windows removed. (C) Details of the sample placed inside the heating element.

samples must be vertically held, as the incident x rays are horizontal. The vertical orientation of the furnace is originally designed for high-temperature microscopy with the sample horizontally held. To keep the liquid sample vertical for XAFS experiment, we have developed a sample cell made of hexagonal BN. The sample is ground into a fine powder and is mixed with hexagonal BN powder and pressed into a disk that is 3.5 mm in diameter. The disk is embedded in the sample holder that is machined from rods of hexagonal BN. The BN matrix, wherein the sample is mixed, serves to sustain the liquid drop in the matrix. Special care is taken to thoroughly homogenize the sample so as to keep the sample disk stable during sample melting, and the x-ray measurements used a large enough beam (approximately 1 mm^2; see below) to average over any remaining inhomogeneities. The high-temperature cell is surrounded by two heating foils (Fig. 2) and covered by the Be window a few millimeters from the heater for thermal radiation shields and then placed inside a vacuum chamber so as to minimize both the radiative and convective heat losses. This provides a high degree of temperature uniformity for the cell and its contents.

Heating is provided by a power supply (10 V and 200 A). The actual sample temperature is determined by a Pt-Pt10%Rh (S type) thermocouple placed just behind the sample, which is located within the BN holder and within a millimeter from the actual sample. The diameter of the sample surface exposed to x ray is approximately 3 mm. The reproducibility and stability of the sample temperature are estimated to be ± 3 K at 1600 K.

III. X-RAY ABSORPTION FINE STRUCTURE SPECTRA ACQUISITION

X-ray absorption fine structure spectra were measured on the Ni K edge (8333 eV) of $Fe_{0.75}Ni_{0.05}S_{0.20}$ and $Fe_{0.75}Ni_{0.05}Si_{0.20}$ at the GeoSoilEnviroCARS bending magnet beamline 13-BM-D, Advanced Photon Source (APS), Argonne National Laboratory. The storage ring was operated at 7 GeV with an ~100 mA current. The x-rays were monochromatized by using a Si(111) double-crystal monochromator. Harmonic rejection was achieved with a Pt-coated mirror pitched at 3 mrad and by detuning the second crystal of the monochromator to reduce the total intensity by ~30%. The Pt-coated mirror was also used to focus the beam in the vertical to ~0.5 mm, and slits were used to define the horizontal beam size to 2.5 mm. Further details of the equipment and x-ray optics of this beamline are described elsewhere.[29,30] The incident x-ray intensity was monitored with a N_2-filled ion chamber. XAFS spectra were measured in the fluorescence mode by using a multielement solid-state Ge detector, which allowed an energy window to be placed around the Ni $K\alpha$ peak at 7480 eV. Due to the high Fe content of the samples and because the Ni K edge is at a higher energy than the Fe K edge, the Fe $K\alpha$ fluorescence (at 6405 eV) was much more intense than the Ni $K\alpha$ fluorescence, and because the solid-state detectors are limited in their total count rate, 150 μm of Al foil were used to preferentially absorb Fe $K\alpha$ over Ni $K\alpha$. XAFS spectra were collected within 15 min by scanning the monochromator energy from 8233 to 8977 eV by using 5 eV steps before the main edge, 0.5 eV steps within ± 20 eV of the main edge, and 0.05 $Å^{-1}$ steps in photoelectron wave number above the main edge. At each energy point, the signals from the ion chamber and the Ni $K\alpha$ for each of the 13 Ge detector elements were recorded for 2 s. Several scans were collected at each temperature and averaged for the analysis.

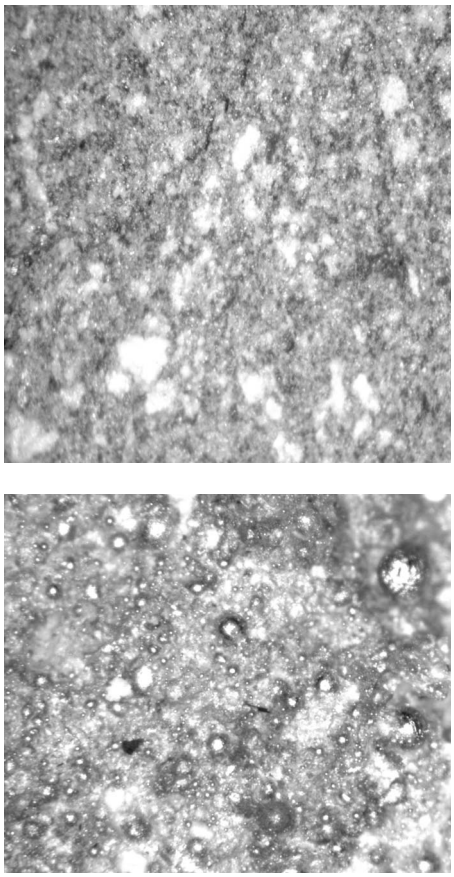

FIG. 3. Photograph of $Fe_{0.75}Ni_{0.05}S_{0.20}$ sample before (top) and after (bottom) melting. The sample stayed intact and did not greatly segregate from its BN matrix.

The two alloy samples were measured at room temperature first then at a series of temperatures of up to 1600 K. The samples were cooled by turning off the power supply, which reached room temperature within several minutes. The samples were optically examined to assess sample integrity. Figure 3 shows the $Fe_{0.75}Ni_{0.05}S_{0.20}$ sample before and after data acquisition. Both the $Fe_{0.75}Ni_{0.05}S_{0.20}$ and the $Fe_{0.75}Ni_{0.05}Si_{0.20}$ samples were clearly melted within the BN matrix, forming small molten balls, as seen in Fig. 3. XAFS recorded on the cooled samples showed similar spectra to those obtained prior to melting, which indicates little or no Ni oxidation during the experiment. There appeared to be some loss of S or Si, as evidenced by the surface color of the Be plate above the molten sample, but these samples stayed intact for several hours during the high-temperature measurements. No evidence of Ni oxidation or reduction was detected either from changes in the x-ray absorption near-edge spectra (XANES) or in the sample color.

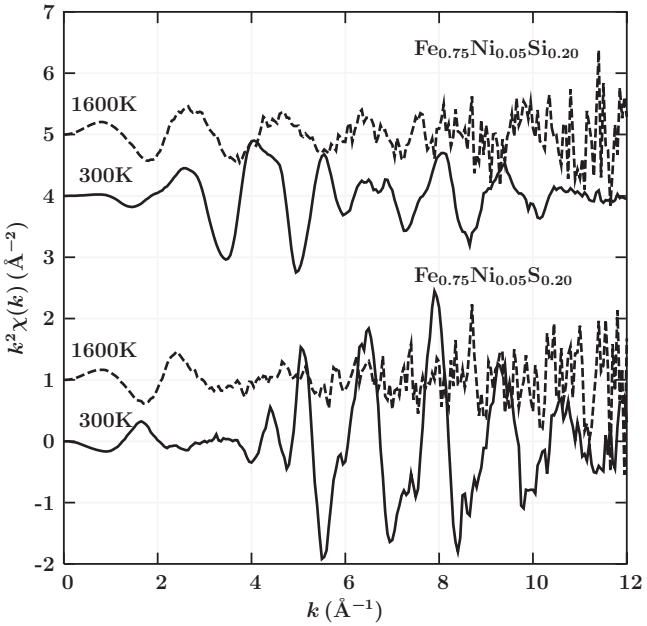

FIG. 4. XAFS $k^2\chi(k)$ for $Fe_{0.75}Ni_{0.05}S_{0.20}$ and $Fe_{0.75}Ni_{0.05}Si_{0.20}$ at room temperature and at 1600 K.

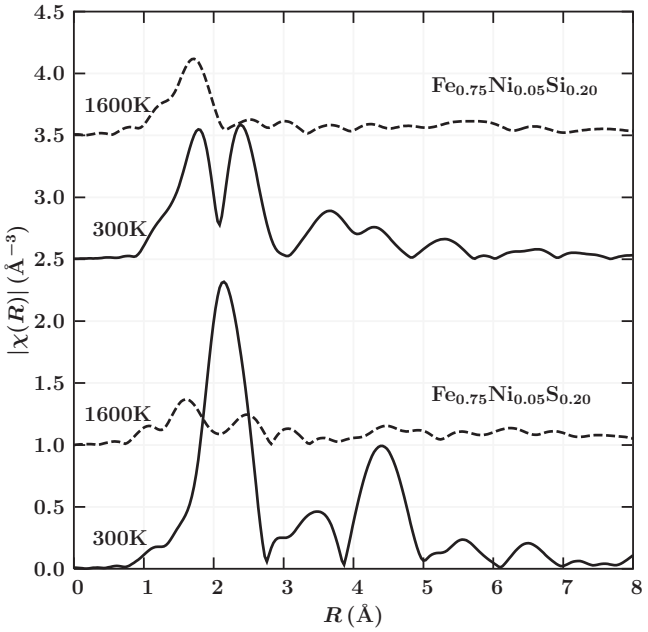

FIG. 5. XAFS Fourier transform $|\chi(R)|$ for $Fe_{0.75}Ni_{0.05}S_{0.20}$ and $Fe_{0.75}Ni_{0.05}Si_{0.20}$ at room temperature and at 1600 K.

IV. X-RAY ABSORPTION FINE STRUCTURE DATA ANALYSIS AND INTERPRETATION

XAFS data processing and analysis were performed with the ATHENA and ARTEMIS programs[31] of the IFEFFIT package.[32] Data were averaged and the slowly varying background was subtracted by using ATHENA, which gives $\chi(k)$ for each temperature. Theoretical models for the XAFS were constructed with FEFF (Refs. 33 and 34) by using crystallographic atomic positions of NiS_2, bcc Fe with Ni substitution, and fcc Fe with Ni substitution. The models were fitted to the data by using ARTEMIS,[31] which also performs an error analysis and calculates the goodness-of-fit parameters.

Figure 4 shows the k^2-weighted $\chi(k)$ XAFS spectra for $Fe_{0.75}Ni_{0.05}S_{0.20}$ and $Fe_{0.75}Ni_{0.05}Si_{0.20}$ at room temperature and at 1600 K. No filtering or smoothing was applied to the data. The oscillations in $k^2\chi(k)$ for $Fe_{0.75}Ni_{0.05}S_{0.20}$ and $Fe_{0.75}Ni_{0.05}Si_{0.20}$ show different amplitudes and frequencies at both room and high temperatures, which indicate that Ni has different local environments in both the solid and melts of these two alloys. These differences, even in the room temperature data, suggest that the Ni coordination is affected by the species of light element in the alloy.

As expected, the XAFS oscillations are greatly damped in the melt phases due to the increased thermal vibrations. Distinct oscillations of up to $k=8$ Å^{-1} are observable for $Fe_{0.75}Ni_{0.05}Si_{0.20}$ even in the melt. This suggests that strong interatomic bonds remain in the $Fe_{0.75}Ni_{0.05}Si_{0.20}$ melt. The larger reduction in the amplitude for the $Fe_{0.75}Ni_{0.05}S_{0.20}$ melt and the changes in the XAFS frequency imply a more significant change in Ni coordination in the melt.

Figure 5 shows $|\chi(R)|$, which is the amplitude of the XAFS Fourier transform of $k^2\chi(k)$, by using a k range from 1 up to 12 Å^{-1} for room temperature spectra and up to 9 Å^{-1} for the 1600 K spectra, and Hanning windows. These k ranges were chosen to obtain a Fourier transform with negligible spurious peaks below the anticipated lowest Ni-S and Ni-Si distances. For $Fe_{0.75}Ni_{0.05}Si_{0.20}$, $|\chi(R)|$ at room temperature shows two strong peaks below 3 Å, which correspond to Ni-Si and Ni-Fe contributions. In the $Fe_{0.75}Ni_{0.05}Si_{0.20}$ melt, the peak at 1.7 Å due to Ni-Si remains, while the peak at 2.3 Å due to Ni-Fe essentially disappears. For $Fe_{0.75}Ni_{0.05}S_{0.20}$, $|\chi(R)|$ at room temperature shows one strong peak at $R\approx 2.1$ Å and higher coordination shells. In the $Fe_{0.75}Ni_{0.05}S_{0.20}$ melt, essentially all these peaks disappear and only a small peak near 1.6 Å remains.

A quantitative analysis of the XAFS performed on the first shell of $|\chi(R)|$ for these spectra provides the qualitative observations above. The data were analyzed in R space, between $R=1.0$ and 3.0 Å, with the theoretical scattering path generated by using FEFF and used with ARTEMIS to determine the best match to the experimental data. The structural parameters shown in Table I are obtained from the ARTEMIS analysis in terms of the first scattering paths of Ni-S, Ni-Si, and Ni-Fe from NiS_2, $NiSi_2$, bcc NiFe, and fcc NiFe at room temperature and at 1600 K, respectively. For the shift in photoelectron energy origin, E_0 was set the same for Ni-S and Ni-Fe, while the coordination number N, distance R, and mean-square displacements σ^2 were treated as free parameters in the fit. Due to the small data range in k and R for the melt data, there was insufficient information[35] to accurately determine the anharmonicity in the Ni coordination shell. Because of this limited data, a more complex modeling of the partial pair distribution function[24,36] $g(R)$ around Ni was not attempted. The results presented here for R may thus have a slight (~0.02 Å) systematic inaccuracy in representing the peak of the $g(R)$ distribution. For the present work, we are satisfied with such distance accuracies, as the typical distances found for Ni-S, Ni-Si, and Ni-Fe differ by much more than this systematic error.

TABLE I. Local structural parameters for Ni in $Fe_{0.75}Ni_{0.05}S_{0.20}$ and $Fe_{0.75}Ni_{0.05}Si_{0.20}$ solid (300 K) and melt (1600 K). The results are derived from FEFF calculations for the XAFS scattering factors and by using the ARTEMIS fitting program. The columns show the sample composition, temperature T, atomic species of the neighbor, number N of bonds, distance R of the bond, mean-square displacement σ^2 in this distance, and goodness-of-fit parameter $\mathcal{R}$. The uncertainties are given in parentheses.

Sample	T (K)	Species	N	R (Å)	σ^2 (Å^2)	R
$Fe_{0.75}Ni_{0.05}S_{0.20}$	300	S	3.2(0.9)	2.36(0.03)	0.010(0.008)	0.01
		Fe	7.6(2.0)	2.49(0.02)	0.009(0.002)	
		Fe	5.6(2.0)	2.82(0.02)	0.017(0.003)	
$Fe_{0.75}Ni_{0.05}S_{0.20}$	1600	S	2.2(1.1)	2.34(0.04)	0.035(0.021)	0.02
		Fe	3.4(2.0)	2.53(0.03)	0.030(0.010)	
$Fe_{0.75}Ni_{0.05}Si_{0.20}$	300	Si	4.1(0.8)	2.26(0.03)	0.004(0.002)	0.03
		Fe	4.1(1.0)	2.23(0.04)	0.011(0.005)	
		Fe	3.1(1.0)	2.82(0.02)	0.007(0.003)	
$Fe_{0.75}Ni_{0.05}Si_{0.20}$	1600	Si	4.1(1.0)	2.41(0.04)	0.031(0.020)	0.07
		Fe	1.8(1.5)	2.52(0.03)	0.017(0.010)	

As shown in Table I, the Ni in $Fe_{0.75}Ni_{0.05}S_{0.20}$ is mainly coordinated by Fe at room temperature, which is consistent with Ni being incorporated into the bcc Fe structure. In the $Fe_{0.75}Ni_{0.05}S_{0.20}$ melt, the very weak XAFS gives lower coordination numbers and higher σ^2 values, which is consistent with Ni being in a "fully melted" metal phase,[21] although there is a suggestion of a small amount of Ni-S bonding persisting in the melt. In contrast, the Ni in $Fe_{0.75}Ni_{0.05}Si_{0.20}$ at room temperature has considerably more Ni-Si near-neighbor bonds and fewer Ni-Fe bonds than would be expected from a random substitution of Ni and Si into the bcc Fe structure. These Ni-Si bonds persist into the melt phase, while the Ni-Fe bonds essentially disappear. The Ni-Si distance is significantly longer in the melt than in the solid phase and somewhat longer than the Ni-Si distance (2.34 Å) found in room temperature $NiSi_2$.[37]

As an additional check on these XAFS results, we use the XANES portion of the XAFS spectra, which provides information about the valence state and local symmetries of the absorbing atom.[38] Figure 6 shows the Ni K-edge XANES spectra of $Fe_{0.75}Ni_{0.05}S_{0.20}$ and $Fe_{0.75}Ni_{0.05}Si_{0.20}$ as well as those of Ni foil, NiO, and NiS_2.[39] It is evident that the XANES spectrum of $Fe_{0.75}Ni_{0.05}S_{0.20}$ at room temperature is fairly similar to that of NiS. On melting, the spectra for $Fe_{0.75}Ni_{0.05}S_{0.20}$ show little change and no sign of significant oxidation—the position of the main absorption edge does not shift to a higher energy as would be expected for Ni^{2+}. Although the XANES spectrum for $Fe_{0.75}Ni_{0.05}Si_{0.20}$ at room temperature is significantly different from that of the sulfide phase, the edge position still suggests that Ni has a metallic character. As for the $Fe_{0.75}Ni_{0.05}S_{0.20}$, the $Fe_{0.75}Ni_{0.05}Si_{0.20}$ shows no sign of oxidation on melting.

V. CONCLUSION

We have described a recently designed high-temperature furnace, which works up to 1600 K and has allowed us to obtain Ni K-edge XAFS spectra in the fluorescence mode for low concentrations (5 wt %) of Ni in $Fe_{0.75}Ni_{0.05}S_{0.20}$ and $Fe_{0.75}Ni_{0.05}Si_{0.20}$ in both solid and melt phases.

We observe relatively strong XAFS oscillations in the $Fe_{0.75}Ni_{0.05}Si_{0.20}$ melt and much weaker oscillations in the $Fe_{0.75}Ni_{0.05}S_{0.20}$ melt. An analysis of the XAFS also shows different local structural environments of Ni atoms in $Fe_{0.75}Ni_{0.05}S_{0.20}$ and $Fe_{0.75}Ni_{0.05}Si_{0.20}$ melts. The Ni in the $Fe_{0.75}Ni_{0.05}S_{0.20}$ solid phase is mainly coordinated by Fe and is consistent with a simple substitution of Ni in the bcc phase of Fe. In contrast, the Ni in $Fe_{0.75}Ni_{0.05}Si_{0.20}$ shows a significant preference for Si at room temperature and persists into the melt. The different Ni coordination environments in the

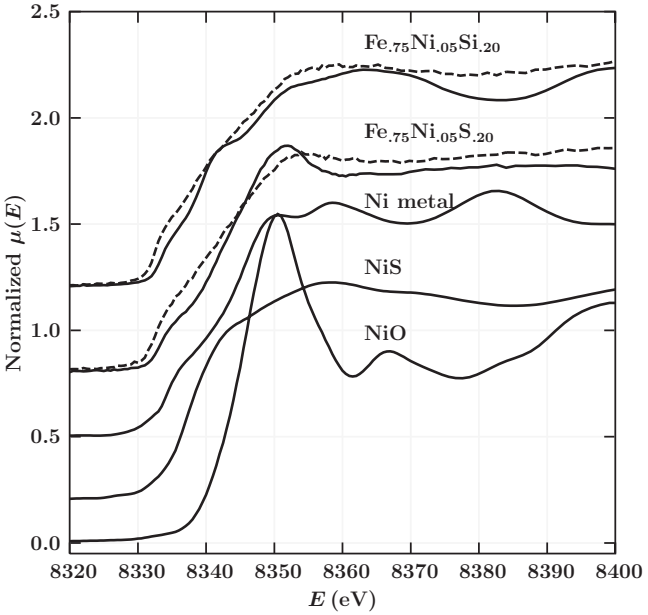

FIG. 6. Ni K-edge XANES of $Fe_{0.75}Ni_{0.05}S_{0.20}$, $Fe_{0.75}Ni_{0.05}Si_{0.20}$, Ni metal, NiO, and NiS. The solid lines show the data collected at room temperature; the white dashed lines show the data at 1600 K.

presence of S and Si in Fe-rich alloys that have compositions similar to those proposed for the earth's core support earlier acoustic measurements in suggesting important differences in the chemical and physical properties of these proposed core compositions.

ACKNOWLEDGMENTS

We thank Y. Wang, G. Shen, and R. Bindu for help with equipment and useful discussions. Portions of this work were performed at GeoSoilEnviroCARS (Sector 13), APS, Argonne National Laboratory. GeoSoilEnviroCARS is supported by the National Science Foundation—Earth Sciences (Grant No. EAR-0622171), the U.S. Department of Energy—Geosciences (Grant No. DE-FG02-94ER14466), and the State of Illinois. The use of the Advanced Photon Source was supported by the U.S. Department of Energy, Office of Science, Office of Basic Energy Sciences, under Contract No. DE-AC02-06CH11357.

*murli@soest.hawaii.edu

[1] R. J. Kinzler, T. L. Grove, and S. I. Recca, Geochim. Cosmochim. Acta **54**, 1255 (1990).
[2] D. A. Snyder and I. S. E. Carmichael, Geochim. Cosmochim. Acta **56**, 303 (1992).
[3] H. K. Mao, Y. Wu, L. C. Chen, J. F. Shu, and A. P. Jephcoat, J. Geophys. Res., [Solid Earth Planets] **95**, 21737 (1990).
[4] O. L. Anderson, Rev. Geophys. **33**, 429 (1995).
[5] J. Badro, G. Fiquet, F. Guyot, E. Gregoryanz, F. Occelli, D. Antonangeli, and M. D'Astuto, Earth Planet. Sci. Lett. **254**, 233 (2007).
[6] J. F. Lin, D. L. Heinz, A. J. Campbell, J. M. Devine, and G. Y. Shen, Science **295**, 313 (2002).
[7] L. Stixrude, in *Molecular Modeling Theory: Applications in the Geosciences*, edited by R. T. Cygan and J. D. Kubicki, Reviews in Mineralogy and Geochemistry Vol. 42 (Mineralogical Society of America, Washington, DC, 2001), pp. 319–343.
[8] P. M. Nasch, M. H. Manghnani, and R. A. Secco, Science **277**, 219 (1997).
[9] M. H. Manghnani, S. S. Fu, R. A. Secco, and P. Nasch, EOS Trans. Am. Geophys. Union **84**, S21E (2003).
[10] G. J. Cuello, R. Fernández-Perea, C. Cabrillo, F. J. Bermejo, and G. Román-Ross, Phys. Rev. B **69**, 094201 (2004).
[11] E. A. Stern and S. M. Heald, in *Handbook of Synchrotron Radiation*, edited by E. E. Koch (North-Holland, New York, 1983), pp. 995–1014.
[12] E. D. Crozier, J. J. Rehr, and R. Ingalls, in *X-Ray Absorption: Principles, Applications, Techniques of EXAFS, SEXAFS, and XANES*, edited by D. C. Koningsberger and R. Prins, Chemical Analysis: A Series of Monographs on Analytical Chemistry and its Applications Vol. 92 (Wiley, New York, 1988), pp. 375–384.
[13] E. D. Crozier, F. W. Lytle, D. E. Sayers, and E. A. Stern, Can. J. Chem. **55**, 1968 (1977).
[14] G. A. Waychunas, G. E. Brown, Jr., C. W. Ponader, and W. E. Jackson, Nature (London) **332**, 251 (1988).
[15] A. Filipponi and A. Di Cicco, Nucl. Instrum. Methods Phys. Res. B **93**, 302 (1994).
[16] K. Tamura, M. Inui, and S. Hosokawa, Rev. Sci. Instrum. **66**, 1382 (1995).
[17] F. Farges, J. P. Itie, G. Fiquet, and D. Andrault, Nucl. Instrum. Methods Phys. Res. B **101**, 493 (1995).
[18] B. Ravel, E. A. Stern, R. I. Vedrinskii, and V. Kraizman, Ferroelectrics **206**, 407 (1998).
[19] J. A. Mavrogenes, A. J. Berry, M. Newville, and S. R. Sutton, Am. Mineral. **87**, 1360 (2002).
[20] G. Jacobs and I. Egry, Phys. Rev. B **59**, 3961 (1999).
[21] E. A. Stern, P. Līvņš, and Z. Zhang, Phys. Rev. B **43**, 8850 (1991).
[22] L. Wenzel, D. Arvanitis, H. Rabus, T. Lederer, K. Baberschke, and G. Comelli, Phys. Rev. Lett. **64**, 1765 (1990).
[23] A. I. Frenkel and J. J. Rehr, Phys. Rev. B **48**, 585 (1993).
[24] A. Filipponi and A. Di Cicco, Phys. Rev. B **52**, 15135 (1995).
[25] *Binary Alloy Phase Diagrams*, edited by T. B. Massalski (American Society for Metals, Metals Park, OH, 1986), Vol. 2.
[26] P. Waldner and A. D. Pelton, Metall. Mater. Trans. B **35**, 897 (2004).
[27] P. Waldner and A. D. Pelton, J. Phase Equilib. **26**, 23 (2005).
[28] O. Ikeda, Y. Himuro, I. Ohnuma, R. Kainuma, and K. Ishida, J. Alloys Compd. **268**, 130 (1998).
[29] M. Newville, S. Sutton, M. Rivers, and P. Eng, J. Synchrotron Radiat. **6**, 353 (1999).
[30] G. Y. Shen, V. B. Prakapenka, P. J. Eng, M. L. Rivers, and S. R. Sutton, J. Synchrotron Radiat. **12**, 642 (2005).
[31] B. Ravel and M. Newville, J. Synchrotron Radiat. **12**, 537 (2005).
[32] M. Newville, J. Synchrotron Radiat. **8**, 322 (2001).
[33] S. I. Zabinsky, J. J. Rehr, A. Ankudinov, R. C. Albers, and M. J. Eller, Phys. Rev. B **52**, 2995 (1995).
[34] A. L. Ankudinov, B. Ravel, J. J. Rehr, and S. D. Conradson, Phys. Rev. B **58**, 7565 (1998).
[35] E. A. Stern, Phys. Rev. B **48**, 9825 (1993).
[36] A. Filipponi, J. Phys.: Condens. Matter **13**, R23 (2001).
[37] R. W. G. Wyckoff, *Crystal Structures*, 2nd ed. (Interscience, New York, 1963).
[38] A. Bianconi, *X-Ray Absorption: Principles, Applications, Techniques of EXAFS, SEXAFS, and XANES* (Ref. 12), Vol. 92, p. 573.
[39] M. Newville, S. A. Carroll, P. A. O'Day, G. A. Waychunas, and M. Ebert, J. Synchrotron Radiat. **6**, 276 (1999).